# Interaction, coalescence, and collapse of localized patterns in a quasi-one-dimensional system of interacting particles

Tommy Dessup, Christophe Coste, and Michel Saint Jean
*Laboratoire "Matière et Systèmes Complexes" (MSC), UMR 7057 CNRS, Université Paris 7 Diderot, 75205 Paris Cedex 13, France*
(Received 25 July 2016; published 13 January 2017)

We study the path toward equilibrium of pairs of solitary wave envelopes (*bubbles*) that modulate a regular zigzag pattern in an annular channel. We evidence that bubble pairs are metastable states, which spontaneously evolve toward a stable single bubble. We exhibit the concept of *topological frustration* of a bubble pair. A configuration is frustrated when the particles between the two bubbles are not organized in a modulated staggered row. For a nonfrustrated (NF) bubble pair configuration, the bubbles interaction is attractive, whereas it is repulsive for a frustrated (F) configuration. We describe a model of interacting solitary wave that provides all qualitative characteristics of the interaction force: It is attractive for NF systems and repulsive for F systems and decreases exponentially with the bubbles distance. Moreover, for NF systems, the bubbles come closer and eventually merge as a single bubble, in a *coalescence* process. We also evidence a *collapse* process, in which one bubble shrinks in favor of the other one, overcoming an energetic barrier in phase space. This process is relevant for both NF systems and F systems. In NF systems, the coalescence prevails at low temperature, whereas thermally activated jumps make the collapse prevail at high temperature. In F systems, the path toward equilibrium involves a collapse process regardless of the temperature.

DOI: 10.1103/PhysRevE.95.012206

## I. INTRODUCTION

There has been a lot of interest in pattern formation in the general context of instabilities in extended systems [1]. In some cases, the patterns are solitons, which means that a complete description of the interactions between localized patterns is available [2]. The complete integrability of nonlinear partial differential equations is seldom, and most often nonlinear patterns are solitary waves but not solitons, so one has to resort to perturbative methods to calculate their interactions [1,3–7]. Moreover, the link between the underlying "microscopic" equations (for instance, the Navier-Stokes equations in the context of convection rolls patterns) and the relevant amplitude equation is difficult to establish quantitatively [1]. In this paper, we study a system with explicit microscopic equations, so all coefficients in the corresponding partial differential equation are known explicitly.

We consider a quasi-one-dimensional system of particles interacting with short-range repulsive potential and transversely confined. There are many practical examples of such a system, like optically confined paramagnetic colloidal particles [8–11], plasma dusts in electrostatic traps [12–16], vortices in supraconductors [17–19], and electrostatically interacting macroscopic beads [20–23]. We have done in Ref. [23] the coarse graining of this discrete system in a consistent fashion and obtained the relevant amplitude equation explicitly, expressing all coefficients in terms of the known interaction potential between the particles.

At a critical transverse confinement, this system has a conformational phase transition which is called the *zigzag transition*. For an even number of particles, the particles are regularly distributed along a line for strong confinement or along a staggered row (zigzag configuration) for a weak confinement. Localized patterns can be observed in these quasi-one-dimensional systems of particles when they are confined in an annular cell [15,22]. For an intermediate confinement, these two phases coexist and the systems present localized patterns, called *bubbles*, of zigzag domains surrounded by particles in line. Indeed, these systems undergo a subcritical pitchfork bifurcation below a critical confinement [23]. For a given number of particles and channel sizes, the bubbles' shapes only depend on the confinement. In a previous article, we have shown that its envelope can be assimilated to a solitary wave which can be calculated in the framework of our nonlinear coarse-grained model [23].

These bubbles are stable in a large range of temperatures [24]. Indeed, under the influence of thermal noise, they diffuse without any distortion of their envelope and the spontaneous splitting of a single bubble never occurs. Note that this solitary wave motion does not correspond to a global displacement of the particles constituting the bubbles. Actually, the bubble envelope moves with respect to the particles. During this displacement the particles are continually reorganized along the solitary wave envelope according to a specific distribution associated to each bubble position. Therefore, bubble motions over large-enough distances induce complete renewal of the entire set of particles participating to the bubble [25]. The change of particles configurations during the bubble motion results in a periodic modulation $\Delta E$ of the potential energy of the system, of period the interparticles distance. This amplitude $\Delta E$ only depends on the transverse confinement. This modulation is a feature of the discrete character of the particles system [25].

By studying the motion of a single bubble at high temperature ($k_BT > \Delta E$), we have evidenced that the bubble diffuses at long times as a free quasiparticle [25]. Indeed, its mean-square displacement depends on time $t$ as $2D_Bt$, where $D_B = k_BT/M_B\gamma$ is the bubble diffusion coefficient, $T$ the thermodynamic temperature, $\gamma$ the dissipation coefficient, and $M_B$ the effective mass of the bubble calculated in the framework of the continuous model [25]. By contrast, at low

 

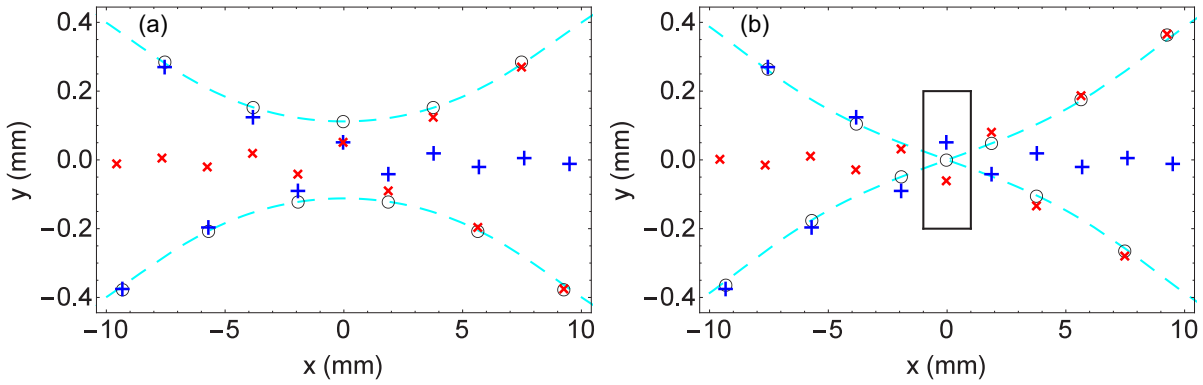


FIG. 1. Schematic representation of the particles configurations for a NF system in (a) and for a F system in (b). In both plots the blue + signs (respectively, red ×) represent the virtual position of the particles in the presence only of the left bubble (respectively, right bubble), the open black circles correspond to the actual position of the particles in presence of both bubbles, and the cyan dashed lines correspond to the analytic transverse displacement field presented Eq. (8). In (b) the black box indicates the location of the *topological defect*.

temperature, the bubble motion is dominated by the potential energy modulation $\Delta E$. The bubble motion might nevertheless still be described as the diffusion of a quasiparticle of mass $M_B$, in an external periodic potential with the same period and the same amplitude as the bubble potential energy [25].

For intermediate confinement, metastable configurations with several bubbles may also be observed. When the system of particles is coupled to a thermal bath, these multibubbles configurations quickly transit toward a simpler system with fewer bubbles, with the thinner bubbles disappearing to the benefit of the wider ones. This seems to be quite a generic process that has already been observed in several nonlinear systems [26–28]. In this paper we focus on the last stage of such a reorganization process, when the system adopts a transient configuration of two identical bubbles before reaching the single bubble equilibrium state.

For discrete systems two kinds of bubble pair configurations have to be considered according the number of particles between the two bubbles. When this number is even, all the particles may organize into a modulated staggered row without any constraint [see Fig. 1(a)]. These systems will be called *nonfrustrated* (NF) systems. By contrast, for an odd number of particles between the bubbles, the relative particles' locations imposed by the two bubbles cannot be simultaneously satisfied and the resulting geometric constraints induce a *topological defect* [see the black box in Fig. 1(b)]. This defect implies that at least one particle cannot take a position compatible with a regular (even if modulated) zigzag pattern. Such systems are therefore called *frustrated* (F) systems. This distinction is mandatory to analyze the bubbles reorganization since the effective force experienced by the bubbles and the processes involved in the bubble pair reorganization differ for NF systems and F systems.

On the other hand, the reorganization of a bubble pair configuration toward a single bubble may involve two distinct mechanisms. In the first process, the bubbles move toward each other, come into contact, and merge into a single bubble. This is the *coalescence process*, which occurs only for NF systems and dominates their dynamics at low temperatures. In the second mechanism, one bubble shrinks and the other one extends, while their positions remain basically constant. We call this process the *collapse process*. It is relevant for NF systems at high temperature and is the only one observed in the reorganization of F systems.

The aim of this article is to discuss in detail the interaction between two bubbles and the processes that lead their reorganization toward a single one. In Sec. II, we calculate the effective interaction between bubbles in the framework of the continuous model, using a simple and nonformal approach (see Appendix B for a formal and rigorous derivation of the bubble interaction which validates this simpler description). We emphasize a remarkable difference between NF and F systems: The bubbles' interaction in a NF system is shown to be attractive, whereas it is repulsive in a F system. The actual motions of interacting bubbles obtained by simulation are described in detail in Sec. III and compared to the theoretical predictions. In particular, we exhibit the influence of the periodic modulation $\Delta E$ on these motions at low temperatures. In Sec. IV, we focus on the coalescence and collapse processes themselves. Then a conclusion summarizes our results in Sec. V. The details of the simulation method are given in Appendix A.

## II. BUBBLES INTERACTION

### A. Normal form of the zigzag bifurcation

We consider $N$ identical point particles of mass $m$ moving on a plane, held in a cell of length $L$ along the $x$ axis with cyclic boundary conditions at the extremities and transversely confined along the $y$ axis by a harmonic potential of stiffness $\beta$. Assuming that $N$ is even, when the confinement becomes smaller than a bifurcation threshold $\beta_{ZZ}$, a chain of equidistant particles undergoes a pitchfork bifurcation toward an homogeneous staggered row of transverse amplitude $2h$. The $i$th particle, which is located at the point $\{x = id, y = 0\}$ with $d = L/N$ before the bifurcation ($\beta > \beta_{ZZ}$) is part of one of the symmetrical patterns $\{id, \pm(-1)^i h\}$ after the bifurcation ($\beta < \beta_{ZZ}$). In this framework, the zigzag bifurcation appears basically as a supercritical pitchfork bifurcation, which implies a soft mode at the bifurcation threshold. Nevertheless, in the thermodynamic limit ($N \to \infty$), the homogeneous patterns (line and zigzag) are translationally invariant, and for finite $N$

with cyclic boundary conditions they are rotationally invariant. In both cases, this invariance implies a soft Goldstone mode. The two soft modes are nonlinearly coupled at the bifurcation, following a mechanism identified in the context of crystal growth [29] and therefore induce a subcritical pitchfork bifurcation.

Indeed, let us consider inhomogeneous patterns, such that the $i$th particle is found at the position $\{x + \phi(x,t),(-1)^i h(x,t)\}$ after the bifurcation, where $\phi(x,t)$ describes the longitudinal deviation from the regular particles distribution and where $h(x,t)$ is the local zigzag height. Introducing the dimensionless distance to the bifurcation threshold $\epsilon$, defined by $\beta \equiv \beta_{ZZ}(1-\epsilon)$, we can expand the energy density near the bifurcation in powers of the small quantity $|\epsilon| \ll 1$. Because of the pitchfork bifurcation, the zigzag height $h$ scales as $\epsilon^{1/2}$. The fields $\phi(x,t)$ and $h(x,t)$ are assumed to be slowly varying functions, and in order to recover the acoustic modes in the low-frequency and long-wavelength limit the slow space and time variables have to scale as $\epsilon^{1/2}$. The scale of the space variable defines the scale of the field $\phi$ as $\epsilon^{1/2}$.

Taking $d$ as the unit distance, the velocity $c_\perp$ of the long-wavelength linear transverse waves as the unit velocity, and $mc_\perp^2$ as the unit energy, a consistent expansion in powers of $\epsilon$ gives the Lagrangian density

$$\mathcal{L} = \frac{1}{2}\left(\frac{\partial h}{\partial t}\right)^2 + \frac{1}{2}\left(\frac{\partial \phi}{\partial t}\right)^2 + \frac{\beta_{ZZ}\epsilon}{2}h^2 - \frac{a_3}{2}\left(h^4 + h^2\frac{\partial \phi}{\partial x}\right) - \frac{1}{2}\left(\frac{\partial h}{\partial x}\right)^2 - \frac{b_3}{2}\left(\frac{\partial \phi}{\partial x}\right)^2 - \frac{a_5}{6}h^6, \quad (1)$$

where all coefficients are explicit positive functions of the interparticles potential [23]. The first two terms are the kinetic energy density, and the remaining terms are the opposite of the potential energy density, $-e_P$. The corresponding field equations are

$$\frac{\partial^2 \phi}{\partial t^2} = a_3 h\frac{\partial h}{\partial x} + b_3\frac{\partial^2 \phi}{\partial x^2}, \quad (2)$$

$$\frac{\partial^2 h}{\partial t^2} = \beta_{ZZ}\epsilon h - a_3\left(2h^3 + h\frac{\partial \phi}{\partial x}\right) + \frac{\partial^2 h}{\partial x^2} - a_5 h^5. \quad (3)$$

Assuming inhomogeneous fields [30], Eq. (2) is readily integrated to give

$$\frac{d\phi}{dx} = -\alpha h(x)^2 \quad \text{where} \quad \alpha \equiv \frac{a_3}{2b_3}. \quad (4)$$

For small-enough interaction range, $\alpha > 2$ and injecting the result (4) into (3) gives a *subcritical* normal form.

The calculations only assume short-ranged interactions between the particles and cyclic boundary conditions in the longitudinal direction. They are thus relevant for plasma dusts in electrostatic traps [12–16] (Yukawa interaction), vortices in supraconductors [17–19], or electrostatically interacting macroscopic beads [20–23] which exhibit the same interaction potential (modified Bessel interaction, see Refs. [19,31]) and optically confined paramagnetic colloidal particles [8–11] (dipolar magnetic interactions). Similar equations have been obtained phenomenologically in Ref. [29] for overdamped dynamics on the basis of symmetry arguments, whereas in our calculation the numerical coefficients in the normal form are explicit functions of the interaction potential [23].

### B. Single bubble description

The *bubbles* are localized zigzag patterns that may be found as stationary solutions which are such that $h(x \to \pm\infty) = 0$. We get

$$h(x) = \frac{h_-}{\sqrt{(1-\chi^2)\cosh^2(\sqrt{-\beta_{ZZ}\epsilon}\,x) + \chi^2}} \quad \text{with} \quad 0 \leqslant \chi < 1, \quad (5)$$

where the parameter $\chi$ and the bubble amplitude $h_-$ are given in Ref. [23]. It is easy to check from (5) that for $x \to \pm\infty$ we have $H(x) \sim \widetilde{H}\exp(\mp\sqrt{-\beta_{ZZ}\epsilon}\,x)$ with

$$\widetilde{H} \equiv \frac{2h_-}{\sqrt{1-\chi^2}}. \quad (6)$$

This asymptotic behavior is generic [6] and is a key point for the calculations of Sec. II D and Appendix B.

From the expression of $h(x)$, using the stress-energy tensor [32] deduced from the Lagrangian density, we can also determine the mass $M_B$ that may be associated to the bubble [25]. It is given by

$$M_B = \int_{-\infty}^{\infty}\left[\alpha^2 h^4 + \left(\frac{dh}{dx}\right)^2\right]dx. \quad (7)$$

The integration may be done with the help of Eq. (5), as shown in Ref. [25]. Qualitatively, as suggested by Eq. (7), we can consider that the effective mass of the bubble increases with its size, the first term accounting for the width of the bubble and the second term for the bubble edges. When the system is put into a thermal bath, the bubbles are found to be stable patterns that behave as quasiparticles, which exhibit a random walk with the diffusion coefficient $D_B = k_B T/(M_B\gamma)$ [25]. Here $T$ is the thermodynamic temperature, $k_B$ the Boltzmann constant, $\gamma$ the dissipation coefficient, and $M_B$ is the quasiparticle mass defined in Eq. (7).

### C. Nonfrustrated and frustrated bubble pair configurations

In the case of a bubble pair configuration, the discrete character of the system of particles imposes to consider the exact location of each particle in the modulated zigzag pattern.

To qualitatively understand this point, let us consider, for instance, a schematic configuration of two zigzag bubbles in a NF system, such as the one displayed in Fig. 1(a). When the bubbles get closer, each bubble induces a displacement in the same direction for evenly indexed particles and in the opposite direction for the oddly indexed ones. Thus the particles between bubbles move away from the confinement axis and eventually take positions satisfying the order imposed by the modulated staggered configuration.

Consider now two zigzag bubbles in a F system, displayed in Fig. 1(b). Now when the bubbles get closer, each bubble induces for each particle a displacement in opposite directions. Therefore, the particle in the middle between the two bubbles stays on the cell axis [see the black box Fig. 1(b)] and appears as a *topological defect* which separates a zigzag pattern

$[y_i = (-1)^i h(x_i)$, say] from a *zagzig* pattern $[y_i = -(-1)^i h(x_i)]$. In this case, the bubble merging is forbidden. Note that in a cyclic channel, there are necessarily two such topological defects, one in each domain between bubbles.

This frustration effect is basically a consequence of the discrete character of the system but may be incorporated in a simple fashion in our continuous description. Indeed, let $\{\phi_L, H_L\}$ be the left bubble, centered at $-D/2$ and $\{\phi_R, H_R\}$ be the right bubble, centered at $+D/2$, with the $x$ origin at the middle of the distance between bubbles. Their superposition is different for NF and F systems. As previously discussed, the sign of the transverse displacements have to alternate strictly for a NF systems (two zigzag bubbles), whereas in contrast a topological defect should separate the two bubbles in F systems [a zigzag bubble (blue +) and a zagzig bubble (red ×), see Fig. 1(b)]. The zagzig bubble may thus be described with transverse displacements of the particles that have opposite signs with respect to the zigzag bubble.

Moreover, we take advantage of the bubble shape asymptotic behavior at large distance (6). Thus, for two bubbles initially at a large distance (such that $D\sqrt{-\beta_{ZZ}\epsilon} \gg 1$), the displacements associated to one bubble are exponentially small at positions for which the displacements associated to the other one are large. In a first approximation [33], one may thus neglect the nonlinear interaction and estimate the longitudinal deviation $\phi(x)$ and the transverse height $h(x)$ describing the whole system as the superposition of single bubble solutions, Eq. (5).

In order to take into account the difference between zigzag and zagzig bubbles, we write the transverse displacement $h(i)$ of the $i$th particle as

$$h(i) = (-1)^i \left[ H_L\left(i + \frac{D}{2}\right) \pm H_R\left(i - \frac{D}{2}\right)\right], \qquad (8)$$

where the sign + corresponds to NF systems and where the sign − corresponds to F systems. Since the field $\phi$ only depends on the square of the transverse displacement [see Eq. (4)], we set

$$\phi(i) = \Phi_L\left(i + \frac{D}{2}\right) + \Phi_R\left(i - \frac{D}{2}\right), \qquad (9)$$

for both F systems and NF systems. The relevance of this description to a bubble pair system is evidenced in Fig. 3 which displays the bubbles configurations and the corresponding calculated envelopes.

### D. Bubbles interaction in the continuous model

The force between the bubbles may be deduced from the potential energy of the whole system. To this end, we inject the ansatzs (8) and (9) into the potential energy density. In principle, one has to take into account that, because of the nonlinear terms, this ansatz is not an exact solution of the dynamical equations (2) and (3). A rigorous calculation of the force between two bubbles is possible, using a general formalism developed by Elphick, Meron, and Spiegel [6]. This calculation is described extensively in Appendix B. We give below a less formal and much simpler presentation, which clearly exhibits the main underlying physical mechanism that is responsible for the force between bubbles.

We simply estimate the potential energy density, neglecting all terms smaller than the product $H_L H_R$ which, because of Eq. (6), is exponentially small for large $D$. We thus obtain

$$e_P = e_P^L + e_P^R \mp \beta_{ZZ}\epsilon H_L H_R \pm a_3(2-\alpha)\left(H_L^3 H_R + H_L H_R^3\right) \pm H_L' H_R' \pm a_5\left(H_L^5 H_R + H_L H_R^5\right), \qquad (10)$$

where the primes denote $x$ derivatives, where we have used Eq. (4) which gives $\Phi'_{L,R} = -\alpha H_{L,R}^2$, and where $e_P^{L,R}$ denotes the potential energy density of the single bubble $\{L, R\}$, which is deduced from (1). The potential energy of the two bubbles is then obtained by integration on the $x$ axis, and after integration by part it reads

$$E_P^{\rm int} = E_P^L + E_P^R \pm \int_{-\infty}^{\infty} \left[-\beta_{ZZ}\epsilon H_L + a_3(2-\alpha)H_L^3 + a_5 H_L^5 - H_L''\right] H_R dx \pm \int_{-\infty}^{\infty} \left[a_3(2-\alpha)H_R^3 + a_5 H_R^5\right] H_L dx. \qquad (11)$$

Since $H_L$ is a solution (5) of (2), the first integral vanishes. In the remaining integral, we get a consistent approximation if we replace $H_L$ by its asymptotic expression $H_L \sim \widetilde{H}\exp[-\sqrt{-\beta_{ZZ}\epsilon}\,(x + D/2)]$. The potential energy now reads

$$E_P^{\rm int} = E_P^L + E_P^R \pm \frac{\widetilde{H}}{\sqrt{-\beta_{ZZ}\epsilon}} e^{-\sqrt{-\beta_{ZZ}\epsilon}D} \times \int_{-\infty}^{\infty} [a_3(2-\alpha)H(w)^3 + a_5 H(w)^5] e^{-w} dw, \qquad (12)$$

where $w = \sqrt{-\beta_{ZZ}\epsilon}(x - D/2)$. This change of variables evidences that the remaining integral is independent of $D$. Because of the translational invariance of the system, the potential energies of each bubble are equal, $E_P^L = E_P^R$, and do not depend on $D$ either.

Once the integration is performed, we obtain the potential energy of interaction between two bubbles as

$$E_P^{\rm int}(D) = \mp 8\sqrt{-\beta_{ZZ}\epsilon}\,\frac{h_-^2}{1-\chi^2} e^{-\sqrt{-\beta_{ZZ}\epsilon}D}, \qquad (13)$$

where the integration constant is such that this energy vanishes when the bubbles are infinitely distant. Then we obtain the force exerted by the left bubble on the right one as

$$F(D) = -\frac{dE_P^{\rm int}}{dD} = \mp \mathcal{F}_0 e^{-\sqrt{-\beta_{ZZ}\epsilon}D}, \quad \text{where}$$
$$\mathcal{F}_0 \equiv 8\beta_{ZZ}|\epsilon|\frac{h_-^2}{1-\chi^2} \geqslant 0. \qquad (14)$$

The most striking result is that the force is attractive for NF systems and repulsive for F systems. Moreover, this expression shows that the intensity of the interaction between bubbles only depends on their distance. All these results are consistent with the rigorous derivation given in Appendix B. An exponentially decreasing interaction has also been calculated for interacting kinks in Ref. [4]. The relevant phenomenon is indeed basically the same, because this latter calculation assumes that the kinks are remote enough for the spatial variations induced by one kink to be small at the location of the other one.

Using the expression of the interacting force, the equation of evolution of the distance between the two bubbles, $D(t)$, is

$$M_B \frac{d^2 D}{dt^2} = \mp 2\mathcal{F}_0 e^{-\sqrt{-\beta_{ZZ}\epsilon}D}. \tag{15}$$

For an attractive interaction, assuming initial conditions such that $D(t=0) = D_0$ and $dD/dt|_{(t=0)} = 0$, we get after integration

$$D(t) = D_0 + \frac{2}{\sqrt{-\beta_{ZZ}\epsilon}} \log\left[\cos\left(\frac{\sqrt{-\beta_{ZZ}\epsilon}\mathcal{F}_0}{M_B e^{\sqrt{-\beta_{ZZ}\epsilon}D_0}}\right)^{1/2} t\right]. \tag{16}$$

The bubbles merge when $D(t_{\max}) = 0$, which happens at time $t_{\max}$,

$$t_{\max} = \left[\frac{M_B \exp(\sqrt{-\beta_{ZZ}\epsilon}D_0)}{\sqrt{-\beta_{ZZ}\epsilon}\mathcal{F}_0}\right]^{1/2} \times \arccos\left[\exp\left(-\frac{\sqrt{-\beta_{ZZ}\epsilon}D_0}{2}\right)\right]. \tag{17}$$

Note that this last result is only approximate, because the calculation assumes a large distance $D(t)$, which is not true during the last stage of the coalescence. For practical calculations, the arccos function is very near $\pi/2$.

### E. Modulation of the interaction potential

An additional potential has to be added to the interaction potential $E_P^{\text{int}}(D)$. Indeed, the reorganization of particles during the bubble displacement along the cell axis induces a small periodic modulation of the potential energy of the system, with a period that is the interparticle distance 1 (since $d$ is taken as the unit length). This modulated potential is a direct consequence of the discreteness of our system, and we have shown in Ref. [25] that it is very well described as a sinusoidal function of amplitude $\Delta E(\epsilon)$ that only depends on the confinement. For a set of two bubbles, the period is 2 and the modulation amplitude is doubled, so the full potential energy of a bubble pair reads

$$E_P(D,\epsilon) = E_P^{\text{int}}(D) + 2\Delta E(\epsilon)\sin\pi D. \tag{18}$$

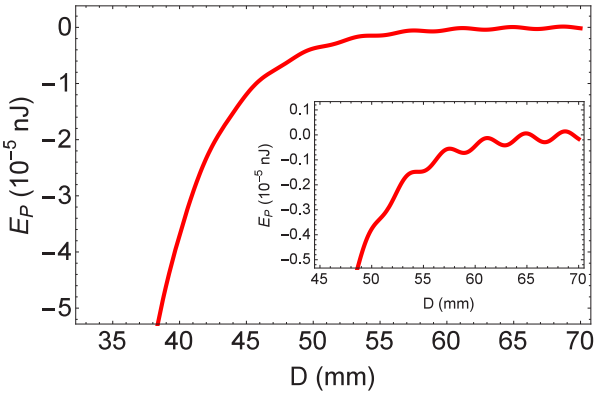


FIG. 2. Plot of the modulated interaction potential energy $E_P$ [in $10^{-5}$ nJ; see Eq. (18)] as a function of the distance $D$ between bubbles (in mm). The inset is a zoom on the large distance behavior that evidences the local minima of energy.

It is plotted in Fig. 2. At small distance, the potential energy is completely dominated by the bubbles interaction potential, but since this latter is exponentially decreasing, the discrete periodic potential dominates at large distance. This is evidenced in the inset of Fig. 2 which shows that, at sufficiently large distance, there are local energy minima such that the bubbles may be trapped in potential wells.

## III. BUBBLE MOTIONS AT ZERO TEMPERATURE

In this section, we focus on the deterministic motions of a pair of bubbles. We compare our theoretical analysis to molecular dynamics simulations at zero temperature. The initial configuration is a metastable bubble pair configuration, with a distance $D_0$ between the two bubbles. Details about this initial configuration are given in Appendix A. Since the interaction force has opposite signs for NF systems and F systems, we discuss these two initial configurations separately.

### A. Bubble motion in NF systems

Let us consider a NF system of two bubbles at $T = 0$ K without dissipation. As soon as their initial distance $D_0$ is such that $d|(dE_P^{\text{int}}/dx)_{D_0}| > \Delta E(\epsilon)$, there is no local energy minimum, and the interaction between the two bubbles is attractive. We display in the left column of Fig. 3 several snapshots of a NF system, taken at increasing time. These plots evidence the attractive interaction and the beginning of the merging of the two bubbles (These snapshots are parts of a movie in the Supplemental Material of this paper, see Ref. [34]). We also plot the ansatz of Eq. (8). We see that this is indeed a very good approximation of the bubble envelope when the distance between the bubbles is large, but that some discrepancy is seen during the merging process, in agreement with the more rigorous approach of Appendix B. The corresponding bubbles trajectories are displayed in Fig. 4. The trajectories are symmetric with respect to the middle of the bubble pair, and each bubble is increasingly accelerated by the attractive force. These observations are consistent with our prediction (14) of an attractive force that only depends on the bubbles distance and that decreases quickly with the distance. On another hand, if $d|(dE_P^{\text{int}}/dx)_{D_0}| < \Delta E(\epsilon)$, which happens when the distance $D_0$ is large enough, there is a local minimum in the bubbles pair energy. Therefore, the bubbles are trapped and oscillate around positions which correspond to local minima of the modulated potential.

In order to check the influence of the initial distance $D_0$ and of the amplitude $\Delta E(\epsilon)$, the bubbles distance $D(t)$ obtained in the simulations is displayed in Fig. 5 as a function of time for four initial distances $D_0$ and for two confinements that correspond to very different amplitudes $\Delta E(\epsilon)$. In the first three plots [Figs. 5(a)–5(c)] $\Delta E(\epsilon)$ is such that no trapping occurs. Thus, the bubbles' motions exhibit the same phenomenology, with a very strong attractive force at small distance and eventually the merging of the bubbles.

The duration of the bubbles motion increases very quickly with the initial distance $D_0$. This is consistent with the result (17), which predicts that the collapse time depends basically exponentially on the distance $D_0$. Moreover, the independence

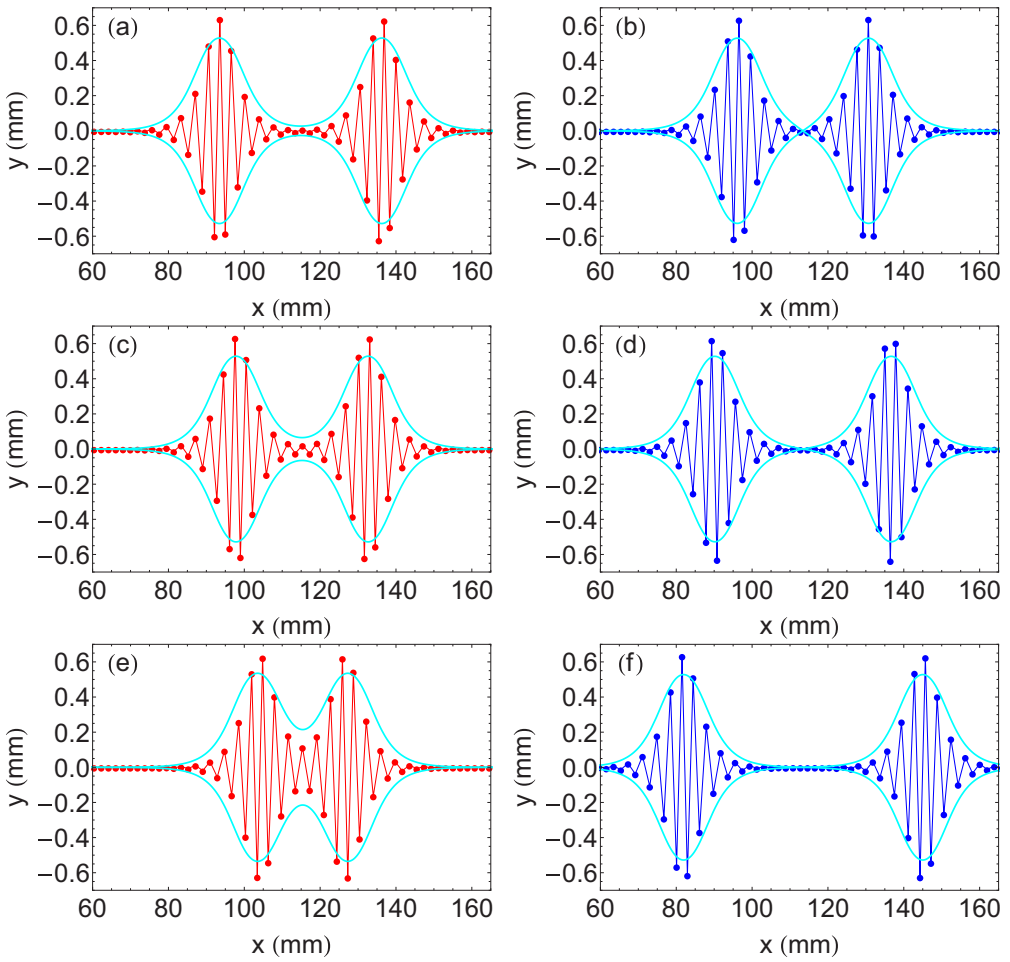


FIG. 3. Snapshots of instantaneous configurations of the particles (both axis in mm) inside a NF system (left plots) and a F system (right plots). For the NF system the configurations are displayed at time 0 s (a), 90 s (c), and 108 s (e). For the F system the configurations are displayed at time 0 s (b), 50 s (d), and 100 s (f). The cyan solid line is the ansatz (8). For both systems there are $N = 128$ particles and the confinement is $\epsilon = 0.05$ (see also the Supplemental Material of this paper [34]).

of the final decrease of $D(t)$ with the initial condition is consistent with a bubble acceleration that depends only on $D$ and not of the velocity, in agreement with expression (14) of $D(t)$. Furthermore, notice that the final decrease of $D(t)$ is independent of the initial bubbles distances. This duration also increases when the amplitude $\Delta E(\epsilon)$ of the periodic potential increases. The most striking effect of the periodic potential is seen in Fig. 5(d). For a given initial distance $D_0$, when $\Delta E(\epsilon)$ is large [here $\Delta E(\epsilon_1) = 7.9\ 10^{-10}$ nJ], the bubbles are stuck in a potential well and always stay around their initial positions. In contrast, with a much smaller $\Delta E(\epsilon)$ [here $\Delta E(\epsilon_2) = 1.0\ 10^{-10}$ nJ] the bubbles are still attracted until their eventual merging. These behaviors cannot be explained by the continuous model, for which there is no threshold of distance which forbids the bubbles motions. Thus, the dynamics described by the continuous model is always faster than that observed in the simulations and the discrepancies are all the more important that the initial distance between bubbles is large enough for the amplitude $\Delta E(\epsilon)$ to be relevant.

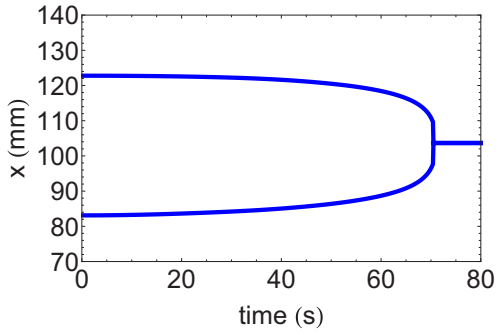


FIG. 4. Positions of the two bubbles (in mm) as a function of the time (in s) for a NF system of $N = 128$ particles, a confinement $\epsilon = 0.05$, and with two bubbles initially separated by a distance of $D_0 = 39.7$ mm.

From the bubbles trajectories, we may calculate the acceleration of the bubbles. The resulting plots are displayed in Fig. 6. When plotted in a log-linear scale [see Fig. 6(b)], the data evidence an exponential decrease of the acceleration with the distance, in qualitative agreement with the theoretical analysis (15).

We can determine the potential energy of a bubble pair, Eq. (18), as a function of the bubbles distance $D$ from the simulation results. With the instantaneous particles positions we can compute easily the interaction energy from the

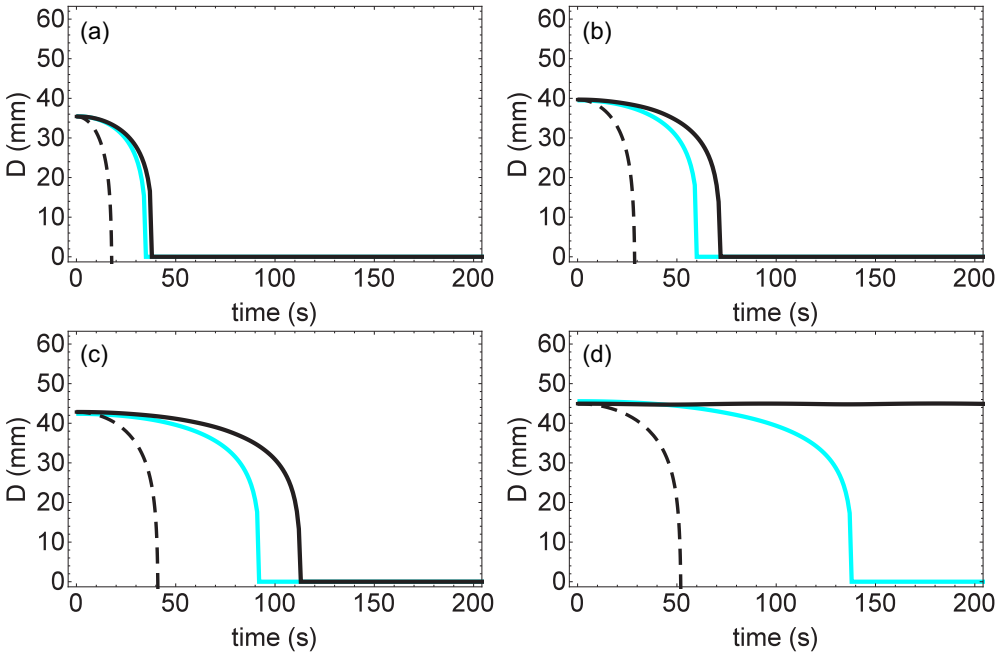


FIG. 5. Plot of the distance $D(t)$ (in mm) between a bubble pair as a function of time $t$ (in s) for a NF system of $N = 128$ particles. For four different initial distances: 35.4 mm (a), 39.7 mm (b), 42.8 mm (c), and 45.6 mm (d). Solid black line: For a confinement $\epsilon_1 = 0.085$ and $\Delta E(\epsilon_1) = 7.9\ 10^{-10}$ nJ. Solid cyan (light gray) line: For a confinement $\epsilon_2 = 0.093$ and $\Delta E(\epsilon_2) = 1.0\ 10^{-10}$ nJ. Dashed black line: Analytical solution, Eq. (16), with a periodic potential energy amplitude $\Delta E(\epsilon) = 0$.

analytical expression of the inter-particles interaction, together with the energy due to the confinement. Figure 7 displays the potential energy as a function of $D$ when two bubbles of a NF-system become closer. At small distance, this energy decreases monotonically with the distance. Even if this section is devoted to motions at zero temperature, let us indicate that for nonzero temperatures, as soon as $k_B T > \Delta E(\epsilon)$, we observe behaviors that are basically the same as those displayed in Figs. 5(a)–5(c). However, at finite temperature, the thermal bath induces random motions of the bubbles, as shown in Fig. 10(a). We can see that the bubbles seem to diffuse independently as long as they are far enough for their interaction to be small compared to the thermal excitation. In contrast, when the bubbles are close enough, the thermal motions become irrelevant so their final motion is basically deterministic and very similar to what it was at $T = 0$ K.

### B. Bubble motion in F systems

The repulsive interaction between bubbles in F systems is evidenced in the right plots of Fig. 3. Initially, the bubbles are very close to the cell center [Fig. 3(a)] and then they repel each other [Figs. 3(d) and 3(f)]. With cyclic boundary conditions, this motion persists until the repulsion becomes strong enough for the bubbles to turn back. Without dissipation this mechanism induces oscillatory trajectories as displayed in Fig. 8(a). These oscillatory motions are also evidenced in a movie provided in the Supplemental Material of this paper, see Ref. [34]. If a small dissipation is introduced, then these oscillatory motions are damped and eventually the bubble positions are such that their final distance is $L/2$ [see Fig. 8(b)].

As for NF systems, the variations of the acceleration with the bubble distance can be determined from the trajectories. The acceleration of a F system as a function of the bubbles

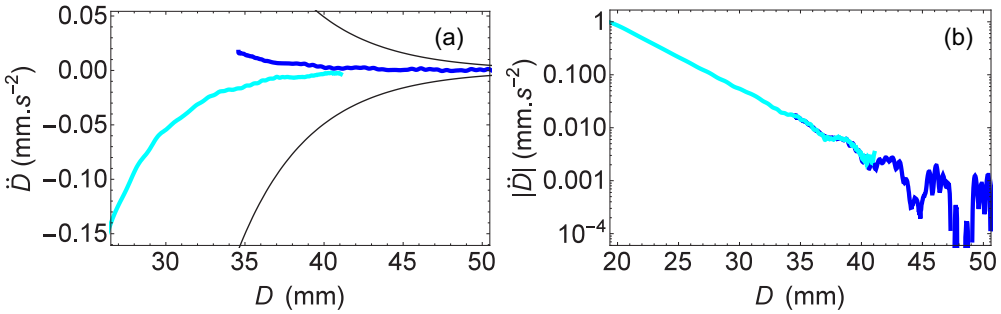


FIG. 6. Acceleration $\ddot{D}$ [in mm s$^{-2}$; (a) linear scale, (b) logarithmic scale] extracted from the trajectories obtained by simulation, such as in Figs. 4 and 3, as function of the distance $D$ between bubbles [in mm; (a) and (b) linear scales]. For both plots the cyan (light gray) curve corresponds to a NF system and the blue (dark gray) curve corresponds to a F system. In (a) the thin black curves correspond to the theoretical expression of the acceleration calculated from Eq. (15). For a system of $N = 128$ particles, $\epsilon = 0.05$, with initial distances of $D_0 = 42.8$ mm for the NF system and of $D_0 = 34.6$ mm for the F system.

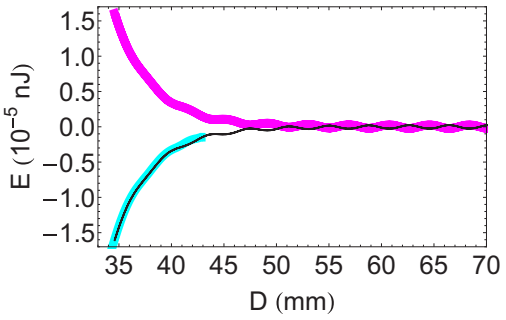


FIG. 7. Plot of the configurational energy (in $10^{-5}$ nJ) as a function of the distance between bubbles (in mm), with the zero energy taken when the bubbles are at infinite distance. The thick cyan (light gray) solid line curve corresponds to the configurational energy of the NF system in Fig. 6, and the thick magenta (darker) solid line corresponds to the F system in Fig. 6. The thin black solid line is the opposite of the F-system energy and is shown to be identical to the NF-system energy.

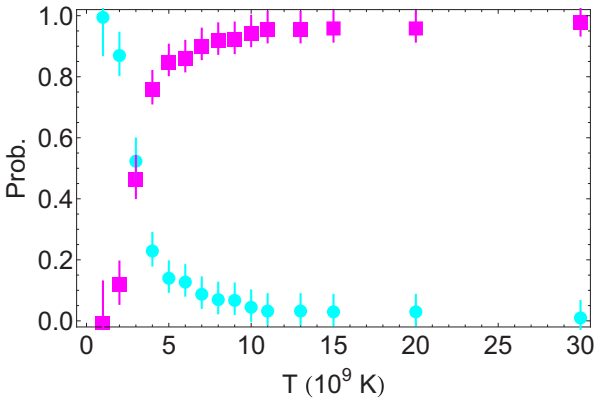


FIG. 9. Probability to observe the reorganization of the bubble pair system via the coalescence process (cyan dots) or via the collapse process (magenta squares) as a function of the temperature ($10^9$ K). For NF systems of $N = 64$ particles and confinement $\epsilon = 0.13$, with bubbles initially separated by $D_0 = 44.1$ mm.

distance $D$ is shown in Fig. 6. It is clear that, when measured at a same distance $D$, the bubbles accelerations in F systems and in NF systems are of opposite signs. These accelerations are shown to have the same absolute value and to exponentially decrease with the distance $D$, which is consistent with Eq. (15) [see Fig. 6(b)].

In Fig. 7 we plot the potential energy of a bubble pair as a function of their distance. This energy increases as the bubble distance decreases, in contrast with NF systems. As expected from Eq. (13), this energy is the opposite of the energy of a NF system. Therefore, the simulations evidence the consistency of our description of a F system by the minus sign in the ansatz (8). Furthermore, the energy of an F system is measured on a larger distance than for NF systems. If the initial condition in an F system is a pair of two close bubbles, then they will gain because of their repulsion a rather large kinetic energy, which allows them to explore the periodic potential energy at large distance.

## IV. REORGANIZATION TOWARD EQUILIBRIUM

### A. The two paths toward the single bubble

The coalescence and the collapse are the two processes by which bubble pair systems can be reorganized toward the equilibrium state of a single bubble. In the coalescence process, the bubbles come into contact and eventually merge together. The required contact is only allowed for NF systems because of the repulsive interaction between bubbles in F systems. In a collapse process, one bubble shrinks in favor of the other one, which becomes the final equilibrium state. During the whole collapse process, the bubbles positions remain constant apart from thermal fluctuations. Since this process does not require any contact between bubbles, it is observed for NF systems and F systems as well.

For the NF system, the relative efficiency of the coalescence and collapse processes only depends on the temperature which controls their respective characteristic times. The coalescence time $\tau_D$ is typically the time required by two bubbles, initially at distance $L/2$, to come into contact by diffusion, the coalescence itself being assumed instantaneous. This time scales as $1/T$. On the other hand, a collapse process requires us to overcome an energetic barrier $\delta U$ in the phase space (see Fig. 13). The characteristic time $\tau_A$ of this thermally activated process is a Kramers's time that scales as $\sqrt{T}\exp(-\delta U/k_B T)$. If $\tau_A > \tau_D$, then the collapse process will always be less efficient than the coalescence process. This is what happens at low temperatures. On the contrary, when $\tau_A < \tau_D$, distant bubbles are more likely to be reorganized by the collapse process. This is what happens at high temperatures.

To quantify the relevance of both processes as a function of the temperature, we have used a statistical approach. For

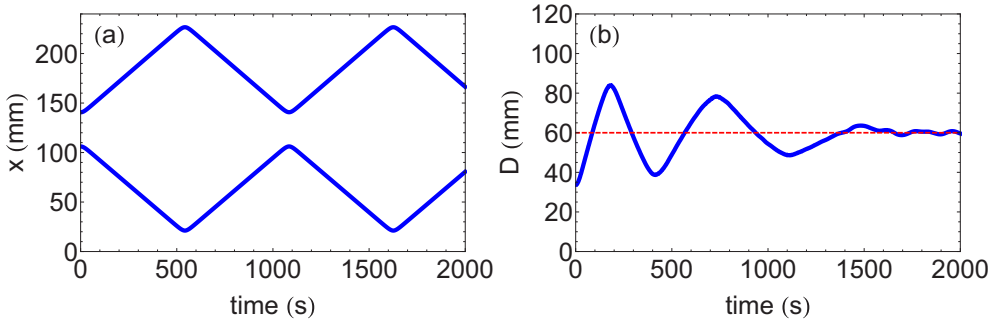


FIG. 8. Positions of the two bubbles (in mm) as a function of the time (in s) for a F system of $N = 128$ particles, a confinement $\epsilon = 0.05$, and with two bubbles initially separated by a distance of $D_0 = 34.6$ mm.

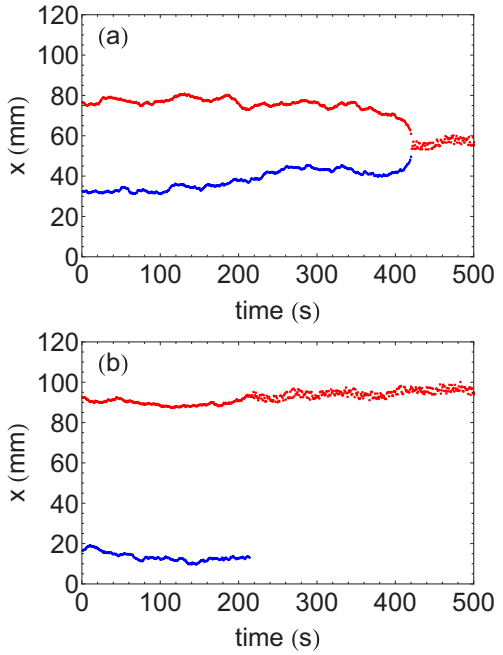


FIG. 10. Positions $x$ of the two bubbles (in mm) as a function of the time (in s) for a NF system of $N = 64$ particles, a confinement $\epsilon = 0.13$, and with two bubbles initially separated by a distance of $D_0 = 44.1$ mm. The temperature is $T = 3.\,10^9$ K and the damping is $\gamma = 1\ \mathrm{s}^{-1}$. (a) Coalescence process. (b) Collapse process. At this temperature both processes are equally likely, see Fig. 9.

each temperature, a large number of simulations have been performed with the same bubble pair initial configuration. We may therefore deduce the probability of each process by counting the number of coalescence or collapse events at each temperature. This probability is plotted as a function of the temperature in Fig. 9. The coalescence is clearly the prevailing process at low temperatures, whereas the system reorganization at high temperatures is mainly due to the collapse process.

### B. Coalescence process

At nonzero temperature, the bubbles behave as quasiparticles in a thermal bath and undergo diffusive motions [24]. A typical set of trajectories for the coalescence of a bubble pair is shown in Fig. 10(a) and should be compared to Fig. 4. The trajectories are noisy at nonzero temperatures because each bubble diffuses in the attractive potential of the other one. When the bubbles are close enough, their motion is leaded by their attractive interaction until they eventually merge together. The last steps of this process are shown in Fig. 11.

The merging process induces a potential energy gain, because the single bubble configuration is more stable than the bubble pair. This potential energy gain is transferred on the vibrational modes of the chain of particles. If the dissipation is small, the central particles exhibit strong transverse oscillations, so the bubbles seem to rebound onto each other (see the movie in the Supplemental Material of this paper [34]). This is illustrated in Fig. 12, which displays the transverse trajectories of two adjacent particles in the middle of the two bubbles. Before the contact, these particles are along the confinement axis. As soon as the bubbles begin to overlap, their transverse positions suddenly increase up to their final positions and oscillate in opposite phase, in agreement with the zigzag geometry. These intermediate states correspond to the lowest energy mode of a single bubble [35]. The amplitude of these oscillations decreases with time because of the redistribution of the kinetic energy on all degrees of freedom of the system and becomes eventually random.

Let us now follow more precisely the evolution of the configurational energy $E(t)$ of the system during its reorganization by coalescence. Such events occur randomly, so measuring $E(t)$ requires many runs of simulations with the same initials conditions. For each simulation, this energy is calculated at each time step, with the coalescence event taken as the time origin. Then an ensemble averaging is performed on all similar events at the same temperature, which gives $E(t)$ for a coalescence process. A typical configurational energy variation is displayed in Fig. 13(a). On this figure, we can identify three distinct steps. The first one is a monotonous energy decrease, which is very slow as long as the bubbles are at large distance, followed by a very quick decrease just before the merging. Then this energy oscillates somewhat, which traces back to the vibrational excitations of the final bubble induced during the coalescence event. Last, the energy reaches the value associated to the stable single bubble configuration. As previously said, the energy excess induced by the coalescence is redistributed as kinetic energy on all the other degrees of freedom of the system, ensuring the total energy conservation. In the Supplemental Material of this paper [34], we display movies of coalescence and collapse

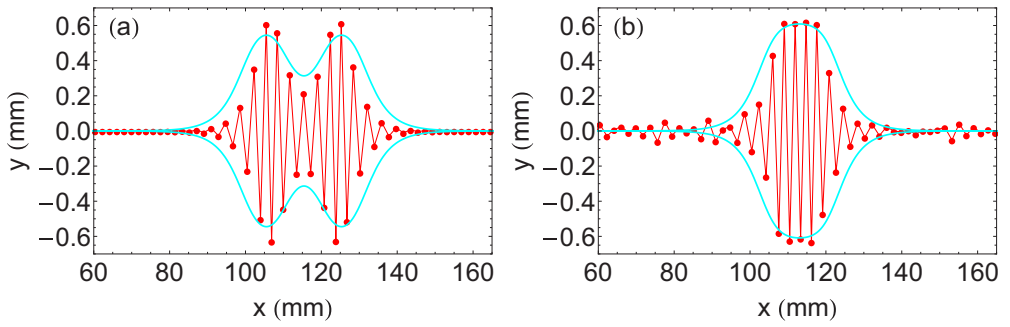


FIG. 11. Two instantaneous configurations (both axis in mm) of the particles inside a NF system taken during the final steps of the coalescence, following the series presented Fig. 3. $N = 128$ particles and $\epsilon = 0.05$. (a) At time 110 s; the cyan solid line is the ansatz (8). (b) At time 340 s; the cyan solid line is the analytic solution (5).

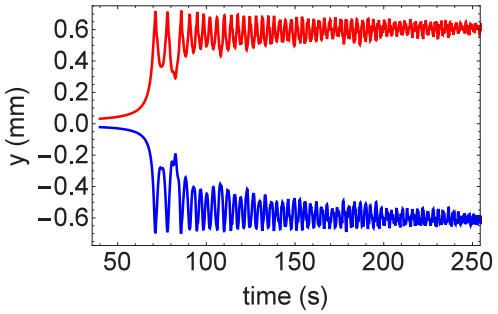


FIG. 12. Transverse positions (in mm) of two successive particles located just at the middle between the two bubbles as a function of the time (in s). For a system of $N = 128$ particles, $\epsilon = 0.05$, at zero temperature and without dissipation.

processes, which show clearly that this excess in potential energy is redistributed on the vibrational modes of the final stable pattern.

### C. Collapse process

Unlike the coalescence which occurs for NF systems only, the collapse processes may happen in NF systems and F systems. An example of the relevant typical bubbles trajectories is presented in Fig. 10(b). Another example of collapse is provided by one movie in the Supplemental Material of this paper, see Ref. [34].

The evolution of the potential energy of a system reorganized by bubbles collapse is shown in Fig. 13(b), with the time origin taken at the end of the collapse. A bubble pair is a metastable state, so before the collapse, the energy remains roughly constant. The collapse event is characterized by a sudden increase of the system energy that reaches a maximum, followed by an eventual quick decrease down to the the energy of the stable single bubble configuration. This characteristic bump defines the energetic barrier $\delta U$, which has to be overcome in this process. It evidences that the collapse is an activated process which therefore prevails at high temperature.

In order to explore the influence of the frustration on this process observed in NFsystems and F systems, we have studied the evolution of the average time $\tau$ required to overcome the barrier as a function of the temperature. Since all simulations

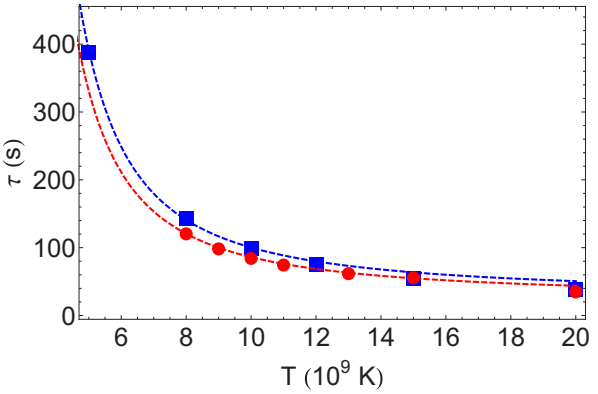


FIG. 14. Plot of the mean time (in s) taken by the system to reorganize toward one bubble via the collapse process as a function of the temperature (in $10^9$ K). The red dots correspond to NF systems and the blue squares correspond to F systems. In both cases $N = 64$ particles, $\epsilon = 0.13$, and the damping constant is $\gamma = 1\ \mathrm{s}^{-1}$.

are done with the same initial condition, the collapse time is the ensemble averaging, at a given temperature, of the times at which a collapse happens in each simulation run, discarding the simulations that exhibit a coalescence process. The plots of this time as a function of temperature are shown in Fig. 14. As expected the average time decreases as the temperature increases. Moreover, this temperature dependence is roughly the same for NF systems and F systems. This suggests that the underlying mechanism of the collapse process, which allows the system to reach its equilibrium state is roughly independent of the existence of a topological defect between the two bubbles.

### D. Final configuration

Let us quickly describe the final bubble itself. The final state of a coalescence process is shown in Fig. 11(b), which shows that it is in very good agreement with the analytic shape (5). More generally, the final single bubble configuration shares the same characteristics for both initial configurations (the bubble pair may be a NF system or an F system) and for both processes (coalescence or collapse). In this way, the final bubble always involves fewer particles in the modulated zigzag phase than the initial state, its height is always slightly smaller and the distance between the aligned particles is larger in the

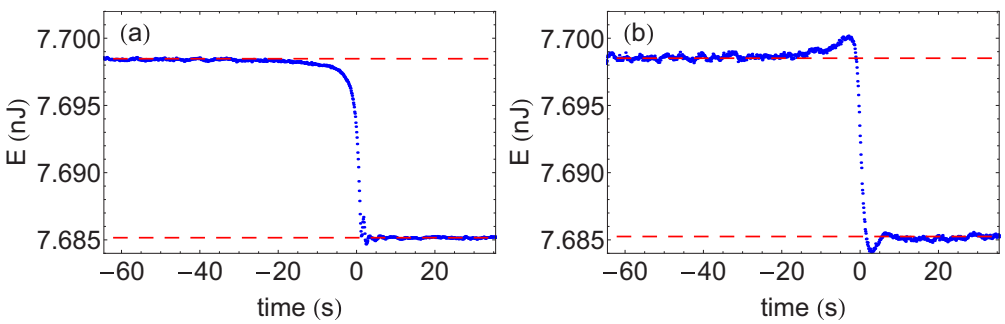


FIG. 13. Instantaneous configurational energy (in nJ) as a function of the time (in s). The configurational energy is averaged over many simulations (see the text for details). In both plots $N = 64$, $\epsilon = 0.13$, the temperature is $T = 10^9$ K and the damping constant is $\gamma = 1\ \mathrm{s}^{-1}$. (a) For a NF system, with the time origin taken at the coalescence event. (b) For an F system, with the time origin taken at the collapse event.

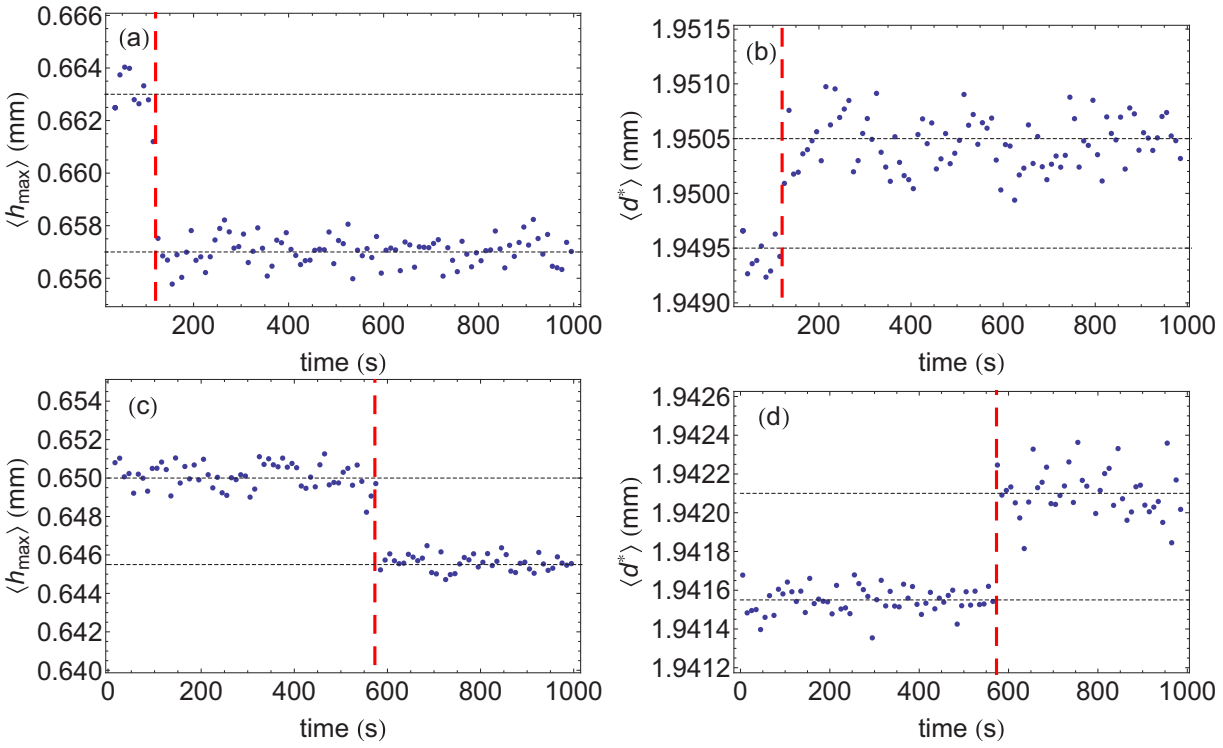


FIG. 15. Left plots: Maximum bubble amplitude $h_{\max}$ (in mm) for a metastable bubble pair and then for the stable single bubble, as a function of time (in s). Right plots: Nearest-neighbors distance $d^*$ (in mm) for particles outside the bubbles, for a metastable bubble pair, and then for the stable single bubble, as a function of time (in s). Top plots for a coalescence process and bottom plots for a collapse process. In each plots the dashed red line indicates the time at which coalescence or collapse happen. For a system of $N = 64$ particles, $\epsilon = 0.15$, at a temperature $T = 5. \times 10^9$ K and with a damping constant $\gamma = 1\ \mathrm{s}^{-1}$.

final state than in the initial state (see Fig. 15). This evidences that the final single bubble is a potential energy minimum, since both the interaction energy and the confinement energy are decreased. The disappearance of a bubble pair in favor of a single bubble has also been observed in systems in which both the energy and the overall mass of the solitary waves are conserved [26–28]. However, we do observe this disappearance in a system which only conserves the total energy. This suggests that this reorganization is quite a generic process.

## V. CONCLUSION

In this article the focus has been put on the path toward equilibrium of nonlinear excitations in discrete systems. The considered excitation are pairs of solitary wave envelopes (*bubbles*) that modulate a regular zigzag pattern in an annular channel with an even number of particles. Such bubbles are observed for an intermediate transverse confinement of this quasi-one-dimensional systems of interacting particles. We observe bubble pairs that are metastable states which spontaneously evolve toward an equilibrium state characterized by a single bubble.

Specific behaviors, not observable in continuous systems have been exhibited due to the underlying discrete character of this system. In particular, we have introduced the concept of *topological frustration* associated to such bubbles pairs. A configuration is said to be frustrated when a regular modulated zigzag phase is impossible between the two bubbles. Using numerical simulations, we have given evidence that when a bubbles pair configuration is nonfrustrated, the bubbless interaction is attractive. In contrast, when the bubble pair is frustrated, the bubbles' interaction is repulsive. We describe a model of interacting solitary wave that takes into account the frustrated or nonfrustrated character of the bubble pair. This model provides all qualitative characteristics of the interaction force: It is attractive for NF systems, repulsive for F systems, and decreases exponentially with the bubbles distance.

For NF systems, the attractive force induces a first path toward equilibrium, as the bubbles move closer and eventually merge as a single stable bubble. This merging process is called *coalescence*. There is another path toward equilibrium, along which one bubble shrinks in favor to the other one, overcoming an energetic barrier in phase space. We call this process the *collapse*. This process occurs for NF systems and F systems as well, whereas the coalescence process, which requires bubbles contact, is specific to NF systems. In the NF systems, the coalescence prevails at low temperatures because the activated jump in phase space is seldom. In contrast, the collapse is the prevailing reorganization process at high temperature. We have monitored the configuration energy during either a coalescence and a collapse process and shown that the collapse is a thermally activated process since an energy barrier has to be overcome just before the collapse.

The key ingredients of our model are a short-ranged interaction and cyclic boundary conditions in the longitudinal direction, which implies an annular shape of experimental setup. The phenomenology described in this paper is thus

expected to be equally relevant for various systems, such as plasma dusts in electrostatic traps [12–16] (Yukawa interaction), vortices in supraconductors [17–19] or electrostatically interacting macroscopic beads [20–23] (in which the short-ranged potential is a modified Bessel interaction, see Refs. [19,31]), and optically confined paramagnetic colloidal particles [8–11] (dipolar magnetic interactions).

## APPENDIX A: NUMERICS

In this paper we simulate the dynamics of $N$ identical point particles of mass $m$ moving on a plane, with a screened electrostatic interaction $U(r) = U_0 K_0(r/\lambda_0)$ of energy scale $U_0$ and of characteristic range $\lambda_0$ between the particles, and with a transverse confinement in a quasi-one-dimensional geometry described by a harmonic potential of stiffness $\beta$. The simulation cell has a longitudinal extent of length $L$ with periodic boundary conditions. The system is connected to a thermal bath accounted for by a damping constant $\gamma$ and by random forces applied on each particle, with the statistical properties of uncorrelated white Gaussian noise. The simulation process involves the numerical resolution of the set of $N$ coupled Langevin equations [36].

The constant $U_0$ determines the energy scales and is such that $U_0/k_B \sim 10^{11}$ K ($k_B$ is Boltzmann constant). In all simulations, we take $\lambda_0 = 0.48$ mm and $d \equiv L/N = 1.875$ mm. Therefore, the coefficient $\alpha$ in Eq. (4) is such that $\alpha > 2$, which ensures the subcriticality of the zigzag bifurcation and, hence, the existence of solitary waves envelope (bubbles) in the system [23,24]. The temperature ranges from $T = 0$ up to a temperature such that the thermal energy is comparable with the characteristic cohesive energies of the system.

Careful attention has been paid to the preparation of the initial bubbles pair configurations. When a bubbles pair emerges in a simulation, we do a fast quenching by reducing the temperature without changing the transverse confinement. To this aim, we simulate the dynamics of the bubbles pair at zero temperature but with a finite dissipation for the system to dissipates its kinetic energy. Eventually, we thus obtained a frozen bubbles pair configuration which can be used as an initial state of the simulations described throughout the paper. We have prepared in such a way several configurations, with various distances between the two bubbles and for the two kinds of bubble pair systems (frustrated and nonfrustated).

## APPENDIX B: RIGOROUS DERIVATION OF THE INTERACTIONS BETWEEN LOCALIZED PATTERNS

In this section, we calculate pertubatively the interaction between two bubbles, using a very general method developed by Elphick, Meron, and Spiegel [6] (EMS). A solitary excitation of a nonlinear partial differential equation in one space variable and one time variable is the solution of an analogous dynamical system. The solitary excitation corresponds to a solution of infinite period of the dynamical system and, hence, to a homoclinic orbit [6,37] that connects a fixed point to itself. Therefore, generically, a solitary wave decays exponentially fast away from its maximum amplitude. The link between the explicit bubble solution (5) and a dynamical system was exhibited in Ref. [23], and Eq. (6) indeed exhibits such asymptotic behavior.

A pair of solitary excitations is not an exact solution, and one has to take into account the complicated nonlinear interaction between the two excitations. However, if they are separated by a large distance $D_0$ ($D_0 \gg 1/\sqrt{-\beta_{ZZ}\epsilon}$), when the amplitude of a bubble is maximum the amplitude of the other one is exponentially small. Therefore, EMS [6] suggest a perturbative calculation, taking $\eta \equiv \exp(-\sqrt{-\beta_{ZZ}\epsilon}\ D_0)$ as a small parameter. Adapting the EMS method to our problem, we seek solutions as

$$\begin{aligned} h &= H\left[x + \frac{D_0}{2} - \psi_L(\tau)\right] \pm H\left[x - \frac{D_0}{2} - \psi_R(\tau)\right] \\ &\quad + \eta R_h(x,\tau) \equiv H_L \pm H_R + \eta R_h, \\ \phi &= \Phi\left[x + \frac{D_0}{2} - \psi_L(\tau)\right] + \Phi\left[x - \frac{D_0}{2} - \psi_R(\tau)\right] \\ &\quad + \eta R_\phi(x,\tau) \equiv \Phi_L + \Phi_R + \eta R_\phi. \end{aligned} \tag{B1}$$

Here $\{H_i(x), \Phi_i(x)\}$, where the index $i \in \{L, R\}$ (left or right) is a stationary solution (5) of Eqs. (2) and (3), such that

$$\mathcal{L}\begin{pmatrix} H_i \\ \Phi_i \end{pmatrix} + \begin{pmatrix} \mathcal{N}_h(H_i,\Phi_i) \\ \mathcal{N}_\phi(H_i,\Phi_i) \end{pmatrix} = \begin{pmatrix} 0 \\ 0 \end{pmatrix}, \tag{B2}$$

with obvious definitions for the linear differential operator $\mathcal{L}$ and for the nonlinear parts $\mathcal{N}_h(H_i,\Phi_i)$ and $\mathcal{N}_\phi(H_i,\Phi_i)$. As in Sec. II D, we describe a NF system by the + sign and a F system by the − sign.

The origin is taken at the middle of the two bubbles, which are initially separated from the distance $D_0$, and since the superposition of the two bubbles cannot be an exact solution, we allow a slow motion of the two bubbles through the functions $\psi_i(\tau)$. We also include two remainder terms, $\eta R_h$ and $\eta R_\phi$. The slow time scale is chosen as $\tau = \eta^{1/2} t$. EMS [6] made a different choice because their underlying model is overdamped, which is not the case for systems (2) and (3).

Then the ansatz (B1) is injected into systems (2) and (3). The expansion of the time derivatives gives

$$\eta^2 \frac{\partial^2 R_h}{\partial \tau^2} + \eta\left(H_L'' \dot{\psi}_L^2 - H_L' \ddot{\psi}_L \pm H_R'' \dot{\psi}_R^2 \mp H_R' \ddot{\psi}_R\right) \tag{B3}$$

and

$$\eta^2 \frac{\partial^2 R_\phi}{\partial \tau^2} + \eta\left(\Phi_L'' \dot{\psi}_L^2 - \Phi_L' \ddot{\psi}_L + \Phi_R'' \dot{\psi}_R^2 - \Phi_R' \ddot{\psi}_R\right). \tag{B4}$$

Since $H_i$ and $\Phi_i$ are functions of only one argument, for the sake of simplicity we write their derivatives with primes. Since $\psi_i$ is a function of $\tau$ only, we write its derivatives with dots.

The next step is to expand the nonlinear terms in power of $\eta$. To this end, following EMS [6], we use what they call the *superposed pulse approximation*. The key point is to notice that at $x = -D_0/2$ (respectively, $x = +D_0/2$) the value of $H_R$ (respectively, $H_L$) is $O(\eta)$. Then we notice that the functions $\mathcal{N}_h$ and $\mathcal{N}_\phi$ are sums of monomials in $h$ and $\phi$ and their derivatives. To carry the expansion in a consistent way, one has to consider that, for $i \neq j$ and a given exponent $a$, $H_i^a H_j^a = O(\eta^a)$ and $H_i^a \Phi_j'^{a/2} = O(\eta^a)$

because $\Phi'_j = -\alpha H_j^2$. Therefore, taking into account that $\{H_i(x), \Phi_i(x)\}$ is a solution of Eq. (5), we get at the leading order

$$\mathcal{H}\begin{pmatrix} R_h \\ R_\phi \end{pmatrix} = -\begin{pmatrix} H''_L\dot{\psi}_L^2 - H'_L\ddot{\psi}_L \pm H''_R\dot{\psi}_R^2 \mp H'_R\ddot{\psi}_R \\ \Phi''_L\dot{\psi}_L^2 - \Phi'_L\ddot{\psi}_L + \Phi''_R\dot{\psi}_R^2 - \Phi'_R\ddot{\psi}_R \end{pmatrix} + \frac{1}{\eta}\begin{pmatrix} a_3\left[6\left(\pm H_L^2 H_R + H_R^2 H_L\right) + H_L\Phi'_R \pm H_R\Phi'_L\right] - 5a_5\left(\pm H_L^4 H_R + H_R^4 H_L\right) \\ \pm a_3(H_L H'_R + H_R H'_L) \end{pmatrix} + O(\eta), \tag{B5}$$

where the linear operator $\mathcal{H}$ is

$$\mathcal{H} = -\mathcal{L} + \begin{pmatrix} 6a_3\left(H_L^2 + H_R^2\right) + a_3(\Phi'_L + \Phi'_R) + 5a_5\left(H_L^4 + H_R^4\right) & a_3(H_L \pm H_R)\frac{\partial}{\partial x} \\ -a_3\left[H'_L \pm H'_R + (H_L \pm H_R)\frac{\partial}{\partial x}\right] & 0 \end{pmatrix}. \tag{B6}$$

For consistency, the correction terms $\eta(R_h, R_\phi)$ in (B1) must be small, so the fields $R_i$ must be finite everywhere. This gives the solvability condition for the perturbative method: By the Fredholm theorem [38], the right-hand member in Eq. (B5) must be orthogonal to the kernel of the adjoint operator $\mathcal{H}^\dagger$, which is defined with the help of the usual inner product for vector functions with bounded support, through the relation

$$\int_{-\infty}^{\infty} \mathbf{P}\cdot(\mathcal{H}\mathbf{R})dx = \int_{-\infty}^{\infty} (\mathcal{H}^\dagger\mathbf{P})\cdot\mathbf{R}dx. \tag{B7}$$

Moreover, the perturbation expansion only requires orthogonality up to $O(\eta)$. We may therefore consider the simpler linear operator

$$\mathcal{H}_L = -\mathcal{L} + \begin{bmatrix} 6a_3H_L^2 + a_3\Phi'_L + 5a_5H_L^4 & a_3H_L\frac{\partial}{\partial x} \\ -a_3\left(H'_L + H_L\frac{\partial}{\partial x}\right) & 0 \end{bmatrix}, \tag{B8}$$

$$\mathcal{H}_R = -\mathcal{L} + \begin{bmatrix} 6a_3H_R^2 + a_3\Phi'_R + 5a_5H_R^4 & \pm a_3H_R\frac{\partial}{\partial x} \\ \mp a_3\left(H'_R + H_R\frac{\partial}{\partial x}\right) & 0 \end{bmatrix}. \tag{B9}$$

Integrating by part, and using the boundary conditions $H_i(\pm\infty) = 0$ and $\Phi'_i(\pm\infty) = 0$, it may be checked that these operators are indeed self-adjoint. Their usefulness comes from the fact that, because of the translational invariance of the underlying equations (2) and (3), we know that the kernel of $\mathcal{H}_i$ is spanned by the vector function $(H'_i, \Phi'_i)$, which may be verified by taking the $x$ derivative of Eq. (B2). Then when $\mathcal{H}^\dagger$ is applied to the kernel of $\mathcal{H}_L$ and $\mathcal{H}_R$, it is easy to see that the result is $O(\eta)$.

Therefore, the consistency of the ansatz (B1) is ensured if we *choose* the functions $\psi_L$ and $\psi_R$ in such a way that the inner products of the right-hand member of Eq. (B5) with the kernels of $\mathcal{H}_L$ and $\mathcal{H}_R$ are both $O(\eta)$. To be specific, let us consider the inner product with the kernel $(H'_L, \Phi'_L)$ of $\mathcal{H}_L$. The terms that involve $\psi_R$ are at least $O(\eta)$ and may thus be discarded. Then the terms $H'_L H''_H$ and $\Phi'_L\Phi''_L$ are exact derivatives, therefore because of the boundary conditions the relevant integrals vanish. Using the relation $\Phi'_L = -\alpha H_L^2$, and integrating by part, we may write the resulting equation as

$$\left[\int_{-\infty}^{\infty}\left(H'^2_L + \Phi'^2_L\right)dx\right]\ddot{\psi}_L = M_B\ddot{\psi}_L = \pm\frac{a_3(\alpha-2)}{\eta}\int_{-\infty}^{\infty} H_L^3H'_R dx \mp \frac{a_5}{\eta}\int_{-\infty}^{\infty} H_L^5H'_R dx, \tag{B10}$$

where we have identified the mass of the bubble with the help of Eqs. (4) and (7).

To calculate the remaining integrals, following EMS [6], we notice that for the left bubble $H_L$ takes significant values for $x \approx -D_0/2$, so we may replace $H'_R$ by its asymptotic value for $x \ll D_0/2$. Therefore, including the arguments of the functions, we get

$$\begin{aligned} \frac{1}{\eta}\int_{-\infty}^{\infty} H_L^n H'_R dx &= \frac{1}{\eta}\int_{-\infty}^{\infty} H\left(x + \frac{D_0}{2} - \psi_L\right)^n \\ &\quad\times \widetilde{H}\sqrt{-\beta_{ZZ}\epsilon}\,e^{\sqrt{-\beta_{ZZ}\epsilon}(x-D_0/2-\psi_R)}dx + O(\eta) \\ &= \widetilde{H}e^{\sqrt{-\beta_{ZZ}\epsilon}(\psi_L-\psi_R)}\int_{-\infty}^{\infty} H(w)^n e^w dw, \end{aligned} \tag{B11}$$

where we have set $w \equiv \sqrt{-\beta_{ZZ}\epsilon}(x + D_0/2 - \psi_L)$ and where we have simplified the last result by $\eta = e^{-D_0\sqrt{-\beta_{ZZ}\epsilon}}$. From the known expression (5) of $H(w)$, we get $M_B\ddot{\psi}_L = \pm\mathcal{F}_0 e^{-\sqrt{-\beta_{ZZ}\epsilon}(\psi_R-\psi_L)}$, where $\mathcal{F}_0$ is defined in Eq. (14). The inner products of the right-hand member of Eq. (B5) with the kernel of $\mathcal{H}_R$ gives a similar equation, $M_B\ddot{\psi}_R = \mp\mathcal{F}_0 e^{-\sqrt{-\beta_{ZZ}\epsilon}(\psi_R-\psi_L)}$.

From these two results, we deduce the time variation of the distance $D$ between the two pulses, which is $D = D_0 + \psi_R - \psi_L$. The physical time $t$ is such that $d^2D/dt^2 = \eta\ddot{D}$, with $\eta = \exp(-\sqrt{-\beta_{ZZ}\epsilon}D_0)$, so

$$M_B\frac{d^2D}{dt^2} = \mp 2\mathcal{F}_0 e^{-\sqrt{-\beta_{ZZ}\epsilon}D}. \tag{B12}$$

This equation evidences an attractive interaction between the bubbles for NF systems and a repulsive interaction for F systems. As of now, we have recovered in a formal but rigorous way, as the solvability condition of our perturbation expansion, the result (14) already given in the text.

[1] M. C. Cross and P. C. Hohenberg, Pattern formation outside of equilibrium, Rev. Mod. Phys. **65**, 851 (1993).

[2] P. G. Drazin and R. S. Johnson, *Solitons: An introduction* (Cambridge University Press, Cambridge, 1989).

[3] M. Oikawa and N. Yajima, Interactions of solitary waves - A perturbation approach to nonlinear systems, J. Phys. Soc. Jpn. **34**, 1093 (1973).

[4] K. Kawazaki and T. Ohta, Kink dynamics in one-dimensional nonlinear systems, Physica A **116**, 573 (1982).

[5] C. Elphick, E. Meron, and E. A. Spiegel, Spatiotemporal Complexity in Traveling Patterns, Phys. Rev. Lett. **61**, 496 (1988).

[6] C. Elphick, E. Meron, and E. A. Spiegel, Patterns of propagating pulses, SIAM J. Appl. Math. **50**, 490 (1990).

[7] C. Elphick, G. R. Ierley, O. Regev, and E. A. Spiegel, Interacting localized structures with Galilean invariance, Phys. Rev. A **44**, 1110 (1991).

[8] G. Piacente, I. V. Schweigert, J. J. Betouras, and F. M. Peeters, Generic properties of a quasi-one-dimensional classical Wigner crystal, Phys. Rev. B **69**, 045324 (2004).

[9] G. Piacente, G. Q. Hai, and F. M. Peeters, Continuous structural transitions in quasi-one-dimensional classical Wigner crystals, Phys. Rev. B **81**, 024108 (2010).

[10] A. V. Straube, R. P. A. Dullens, L. Schimansky-Geier, and A. A. Louis, Zigzag transitions and nonequilibrium pattern formation in colloidal chains, J. Chem. Phys. **139**, 134908 (2013).

[11] Christian Marschler, Jens Starke, Mads P. Sørensen, Yuri B. Gaididei, and Peter L. Christiansen, Pattern formation in annular systems of repulsive particles, Phys. Lett. A **380**, 166 (2016).

[12] B. Liu and J. Goree, Phonons in a one-dimensional Yukawa chain: Dusty plasma experiment and model, Phys. Rev. E **71**, 046410 (2005).

[13] A. Melzer, Zigzag transition of finite dust clusters, Phys. Rev. E **73**, 056404 (2006).

[14] T. E. Sheridan, Dusty plasma ring model, Phys. Scr. **80**, 065502 (2009).

[15] T. E. Sheridan and K. D. Wells, Dimensional phase transition in small Yukawa clusters, Phys. Rev. E **81**, 016404 (2010).

[16] T. E. Sheridan and A. L. Magyar, Power law behavior for the zigzag transition in a Yukawa cluster, Phys. Plasmas **17**, 113703 (2010).

[17] A. J. Drew, M. W. Wisemayer, D. O. G. Heron, S. Lister, S. L. Lee, A. Potenza, C. H. Marrows, R. M. Dalgliesh, T. R. Charlton, and S. Langridge, Using spin-polarized neutron reflectivity to probe mesoscopic vortex states in a pb thin-film superconductor, Phys. Rev. B **80**, 134510 (2009).

[18] R. B. G. Kramer, G. W. Ataklti, V. V. Moshchalkov, and A. V. Silhanek, Direct visualization of the campbell regime in superconducting stripes, Phys. Rev. B **81**, 144508 (2010).

[19] Q. Le Thien, D. McDermott, C. J. Olson Reichhardt, and C. Reichhardt, Orientational ordering, buckling, and dynamic transitions for vortices interacting with a periodic quasi-one-dimensional substrate, Phys. Rev. B **93**, 014504 (2016).

[20] J.-B. Delfau, C. Coste, and M. Saint Jean, Transverse single-file-diffusion near the zigzag transition, Phys. Rev. E **87**, 032163 (2013).

[21] J.-B. Delfau, C. Coste, and M. Saint Jean, Noisy zigzag transition, fluctuations, and thermal bifurcation threshold, Phys. Rev. E **87**, 062135 (2013).

[22] T. Dessup, T. Maimbourg, C. Coste, and M. Saint Jean, Linear instability of a zigzag pattern, Phys. Rev. E **91**, 022908 (2015).

[23] T. Dessup, C. Coste, and M. Saint Jean, Subcriticallity of the zigzag transition: A nonlinear bifurcation analysis, Phys. Rev. E **91**, 032917 (2015).

[24] T. Dessup, C. Coste, and M. Saint Jean, Hysteretic and intermittent regimes in the subcritical bifurcation of a quasi-one-dimensionnal system of interacting particles, Phys. Rev. E **93**, 012105 (2016).

[25] T. Dessup, C. Coste, and M. Saint Jean, Thermal motion of a nonlinear localized pattern in a quasi-one-dimensional system, Phys. Rev. E **94**, 012217 (2016).

[26] R. Jordan and C. Josserand, Self-organization in nonlinear wave turbulence, Phys. Rev. E **61**, 1527 (2000).

[27] B. Rumpf and A. C. Newell, Localization and coherence in nonintegrable systems, Physica D **184**, 162 (2003).

[28] B. Rumpf, Stable and metastable states and the formation and destruction of breathers in the discrete nonlinear Schrödinger equation, Physica D **238**, 2067 (2009).

[29] B. Caroli, C. Caroli, and S. Fauve, On the phenomenology of tilted domains in lamellar eutectic growth, J. Phys. I France **2**, 281 (1992).

[30] For homogeneous fields, the density is a constant and the only physically consistent solution of (2) is $d\phi/dx = 0$, so the normal form (3) remains *supercritical*.

[31] P. Galatola, G. Coupier, M. Saint Jean, J.-B. Fournier, and C. Guthmann, Determination of the interactions in confined macroscopic wigner islands: Theory and experiments, Eur. Phys. J. B **50**, 549 (2006).

[32] H. Goldstein, *Classical Mechanics* (Addison Wesley, Reading, MA, 1980).

[33] In the rigorous calculation, the nonlinear interaction between the two bubbles is taken into account perturbatively in a consistent way, see Appendix B and Ref. [6].

[34] See Supplemental Material at http://link.aps.org/supplemental/10.1103/PhysRevE.95.012206 for four movies of bubbles motions.

[35] J.-B. Delfau, C. Coste, and M. Saint Jean, Enhanced fluctuations of interacting particles confined in a box, Phys. Rev. E **85**, 041137 (2012).

[36] J.-B. Delfau, C. Coste, and M. Saint Jean, Single file diffusion of particles with long-ranged interactions: Damping and finite size effects, Phys. Rev. E **84**, 011101 (2011).

[37] E. Infeld and G. Rowlands, *Nonlinear Waves, Solitons and Chaos* (Cambridge University Press, Cambridge, 1990).

[38] P. Manneville, *Dissipative Structure and Weak Turbulence* (Academic Press, New York, 1990).